Journal of Materials Chemistry A

Accepted Manuscript

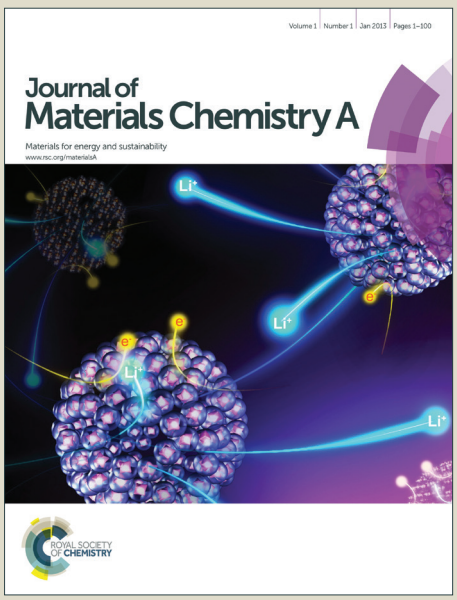

ROYAL SOCIETY OF CHEMISTRY

www.rsc.org/materialsA

Journal Name

RSCPublishing

ARTICLE

Structure and crystallinity in water dispersible photoactive nanoparticles for organic solar cells

Cite this: DOI: 10.1039/x0xx00000x

E. B. L. Pedersen[a], M. C. Pedersen[b], S. B. Simonsen[a], R. G. Brandt[c] , A. P. L. Böttiger[a], T. R. Andersen[a], W. Jiang[d], X. Zhiyuan[d], F. C. Krebs[a], L. Arleth[b] and J. W. Andreasen[a].

Received 00th January 2012,
Accepted 00th January 2012

DOI: 10.1039/x0xx00000x

www.rsc.org/

Water based inks would be a strong advantage for large scale production of organic photovoltaics. Formation of water dispersible nanoparticles produced by the Landfester method is a promising route to achieve such inks. We provide new insights into key ink properties for poly(3-hexylthiophene) (P3HT) and [6,6]-phenyl-C61-butyric acid methyl ester (PCBM) nanoparticles such as internal structure and crystallinity of the dispersed nanoparticles and the previously unreported drastic changes that occur when the ink is cast into a film. We observe through Transmission Electron Microscopy (TEM) and small angle X-ray scattering (SAXS) that the nanoparticles in dispersion are spherical with nano domains of P3HT – partly crystalline. When wet processed and dried into films the nanoparticles lose their spherical shape and become flattened to oblate shapes with a large aspect ratio. Most particles are observed to have a diameter 13 times of the particle height. After casting to a film the crystal domains adopt a preferred orientation with the majority of the nano crystals (68%) with face-on orientation to the substrate. We propose that low substrate surface energy is responsible for particle deformation and texturing.

Broader context

Polymer solar cells have demonstrated power conversion efficiencies comparable to what can be achieved with other thin-film technologies, but some issues with respect to environmental impact remain to be addressed. Photoactive nano-particles in aqueous dispersion have been envisioned as an effective way to do away with the use of toxic and environmental harmful solvents in the coating process of polymer solar cells. Preforming the donor/acceptor blend in nanoparticles that are dispersed in water allows for use of only aqueous or alcohol-based inks for coating, while at the same time providing a means of controlling the nano-structure of the heterojunction. We show that the nano-particles are very sensitive to the type of coating method and substrate surface energy, and that an otherwise optimal nano-structure may be compromised during coating by phase separation. Our results indicate that focusing the development effort on other types of stabilizing surfactants may provide the means to control phase separation and thus the formation of optimal nano-structure in roll-to-roll coated, environmental friendly polymer solar cells.

Introduction

Looking for alternative energy sources to reduce human dependence on fossil fuels and to promote a move towards societies powered by clean renewable energy, solar energy has by far the greatest potential[1,2]. Traditional silicon based solar technology is not competitive in energy price and face additional challenges in long energy payback time and recycling issues[3]. Organic PhotoVoltaics (OPV) is a promising group of solar technologies based on thin films of organic molecules, and has advantages of low energy payback time due to fast scalable roll-to-roll processing, use of small amounts of abundant materials in thin films and low temperature production[4,5]. Recently, the large scale deployment of organic solar cells has been demonstrated showing an advantage in scalability, but also highlighting the need for further research[6].

One of the areas of development is the active material itself. The active layer in OPV is typically cast from toxic chlorinated organic solvents. Production can be improved by switching to water based inks and thereby not having to deal with toxic and flammable fumes. Water based inks can also be coated simultaneously with interface layers like PEDOT:PSS as demonstrated through double slot dye coating[7].

There has been work on making water-soluble polymers which unfortunately have shown low energy conversion effeciency[8]. Another approach is to use a surfactant to preprocess the polymers into water dispersible nanoparticles with the Landfester method[9]. This method also causes a drop in energy conversion efficiency[10], indicating the challenge in taking proven materials and transforming them into water based inks. If successful, a Landfester method would

reduce the chloroform use to 45% of current solution based methods, and with the addition of a condenser, a closed loop system can be formed, where the chloroform is recycled and there is no ongoing consumption of chloroform.

Poly(3-hexylthiophene) (P3HT) and [6,6]-phenyl-C61-butyric acid methyl ester (PCBM) is a well-established active layer mixture. Surfactant free P3HT-PCBM nanoparticles have also been pursued[11] even with a high power conversion efficiency of 4%[12]. However, the high efficiency is not achieved by coating from water dispersion but with ethanol as the dispersion medium. The long term stability of these alcoholic nanoparticle dispersions has yet to be demonstrated but more importantly there is a need to understand the mechanism of film formation and morphology evolution from these nanoparticles to facilitate the development of water based inks that yield efficient performance when processed into solar cells. This calls for additional characterization of the nanoparticles themselves and the layers formed from them.

Dastoor *et al.* performed a number of studies on OPV relevant nanoparticles and found a number of interesting effects[11,13–16]. The ideal thickness of the film is quite thin (but comparable to bulk material), about 300 nm, and with careful annealing the surfactant appears to be removed from the connecting interfaces[15]. The internal structure of large Landfester particles (on the order of 150 nm diameter) has been found to be a core shell structure that grows upon annealing[13–16]. The large particles are a good model system but undesirable for application in OPV because they limit the active layer to only 1-2 particles in thickness, which yield very inhomogeneous layers, poor films and a high risk of electric short circuits when processed into complete final devices. In practice the particle size in water based inks used for fabricating devices are on the order of 20-50 nm in radius[15] and so far there only exist rough qualitative assessments regarding their internal structure[17].

Direct microscopy methods such as Scanning Transmission X-ray Microscopy have difficulties reaching resolutions of sub 10 nm even though development of soft X-ray ptychography has enabled 5 nm spatial resolution and 18 nm chemical resolution[18]. Scattering techniques such as Small Angle X-ray Scattering (SAXS) are capable of resolving smaller length scales but probes the entire illuminated population of nanoparticles. With such a technique no information of the individual particles is gained, but rather ensemble information. Furthermore, a suitable structural model must be formulated to extract information from the SAXS patterns. In the literature, there already exists a number of structural models for nanoparticles and their internal structure such as homogenous spheres and core-shell particles[19]. There has also been formulated general models to describe complex internal structures such as the Teubner-Strey description of microemulsions[20]. In conclusion, SAXS appears as an attractive method to quantify the average internal structure of Landfester nanoparticles relevant for OPV.

Another parameter which has so far not been touched upon in the analysis of OPV relevant nanoparticles is crystallinity. Compared to a bulk material the confinement of the polymer can reduce the crystallinity as seen in other systems[21], where also sonication[22] and surfactant parameters[23] affect crystallinity. This is particularly interesting in the context of OPV where materials crystallinity has been found to correlate with device current[24] – a parameter normally reduced in nanoparticle devices[16]. Crystallinity can easily be measured with X-ray diffraction. From X-ray diffraction structural information like the crystal domain size[25,26] and crystal orientation can be extracted. P3HT is in particular known to assume two orientations either face-on (side chains aligned parallel to the substrate) or edge-on (side chains aligned perpendicular to the substrate). With the crystal domains confined in the spherical nanoparticles one would expect random orientation of the crystal domains.

In this manuscript we use SAXS to characterize the internal structure of P3HT-PCBM Landfester particles with relevant diameters on the order of 20 nm for the first time. Furthermore, we investigate crystallinity of the particles in the aqueous dispersion and when cast into film and dried, supplemented by Atomic Force Microscopy (AFM) measurements to confirm drastic structural changes in the particles during casting and drying.

Results and discussion

In the following sections we first introduce the characterization of the nanoparticles in water dispersion. Afterwards we present the results for the film formation and link it to the characterization of internal particle structure.

Nanoparticles in dispersion

For the water based nanoparticle inks, the structural characterization falls into three categories, the particle size distribution, internal size distribution and crystal domain size. For the majority of these efforts we will study P3HT:PCBM 1:1 (mass ratio) Landfester particles. The particle size distribution is characterized with dynamic light scattering (DLS), transmission electron microscope (TEM) and SAXS using different models for internal structure as shown in figure 1. Both SAXS models and the TEM measurements agree on the size distribution as a log-normal distribution with the median around 8 nm. The samples contain a small fraction of aggregated nanoparticles in the dispersion, which complicates the DLS measurements. A traditional second order cumulant analysis fit to the correlation function gives a size distribution with an average hydrodynamic particle radius that is about 10 nm larger than observed through the other methods. However, a double exponential fit reveals two main populations: 97% volume fraction with a radius of 8.9 nm (in agreement with the SAXS and TEM measurements) and 3% volume fraction with a radius of around 40 nm. The two populations of the double exponential fit is consistent with the findings through a free form Contin analysis (results not shown). The DLS size distribution extracted with second order cumulant analysis try to accommodate both populations, which leads to an overestimation of particle size and poor fits to the correlation function. Landfester particle sizes reported only based on DLS using second order cumulant analysis should therefore be reconsidered as the true particle sizes might be smaller.

Crystallinity. In X-ray studies of the dispersed nanoparticles, we observe the P3HT *100* reflection, corresponding to lamellar packing[27] as shown in figure 2A. We tested the crystal behaviour in 3 kinds of nanoparticles and found a peak at 0.39 $Å^{-1}$ in particles of pure P3HT and 0.38 $Å^{-1}$ in particles containing P3HT:PCBM 1:1 by weight (figure 2). With P3HT:PCBM 1:7 particles (12.5 weight % P3HT) no crystal domains are formed. Similar observations have been reported for bulk mixtures with minimum P3HT fractions from 10 to 30% required for formation of crystalline P3HT domains[28,29]. From the width of the diffraction peak the average crystal domain size is determined by the Scherrer equation, as shown in **table 1**. With a P3HT *100* lattice spacing of 1.60 - 1.64 nm the number of molecules in the average crystalline domain is found to be about 3 molecules in the mixed particles and 5 molecules in the pure P3HT particles, along the *100* direction. The integrated intensity of the P3HT *100* peak decreases by a factor of 2.7 when mixed with PCBM, relative to the P3HT:PCBM 1:1 blend, whereas a factor of 2 would be expected, just considering concentration.. In combination with the observation of reduced P3HT domain size in the blend, this is taken as an indication of PCBM interfering with the crystallization of P3HT.

The water dispersed nanoparticles already contain nanometer-sized crystal domains and are therefore to some degree already phase separated unlike the solution based inks. Optimal device morphology requires a high degree of intermixing of active layer materials, since the exciton diffusion length is only about 10 nm[30]. Phase separation in the water-based ink can be problematic, because annealing can increase the domain size significantly above the exciton diffusion length. Domain sizes in annealed Landfester nanoparticles have previously been shown to increase above the initial particle size[16]. Devices cast from solution based inks have also shown decreases in power conversion efficiency after long annealing times (60 min) due to phase separation of the active layer material[31].

Internal structure. To investigate the precise internal nanoparticle structure we employ a more detailed modelling of the full SAXS patterns for the particles shown in figure 2. For this purpose, we developed two scattering models of mixtures of P3HT:PCBM particles: A geometric core-shell model as previously reported[19] and a more abstract Teubner-Strey model which describe internal structure by a characteristic domain size and correlation length[20]. The fundamental mathematical expression is the form factor amplitude of a sphere (see e.g. Pedersen[32] for details on establishing geometric models of small-angle scattering). It is used to describe the scattering from the core and shell of the particles, the surfactant layer describing the hydrophobic SDS-tail, and an outer layer describing the hydrophilic SDS-headgroups (SDS = Sodium dodecyl sulfate).

In the model, we implement so-called molecular constraints in the model in order to minimise the number of refined parameters in the structural model. As an example, the scattering length density of the SDS-layers is kept consistent with the molecular properties of SDS rather than refining this quantity from the data.

We implemented a polydispersity of the particles in our model in order to accommodate the inherent dispersion in the particle size arising from the applied self-assembly procedure. This was done by numerical integration over a log-normal volume-weighted distribution of the radius of the core-shell-structure describing the P3HT:PCBM particles.

As shown in figure 2, the simple model for polydisperse core-shell-like particles fails to adequately reproduce the features of the data. For this reason, we instead use a homogenous sphere and included a contribution to the scattering arising from an emulsion-like domain structure as described by Teubner and Strey[20].

Furthermore, in order to fit the 100-peak of P3HT, a Gaussian was added to the final model in order to capture the crystalline diffraction from the P3HT.

Mathematically, we can write the final model as:

$$\begin{aligned} I(q) &= I(q)_{\text{Teubner-Strey}} + I(q)_{\text{Diffraction peak}} + I(q)_{\text{Particles}} \\ &= \frac{C_{\text{Teubner-Strey}}}{a_2 + c_1 q^2 + c_2 q^4} + C_{\text{Diffraction peak}} \cdot e^{-\frac{(\mu_D - q)^2}{2{\sigma_D}^2}} \\ &+ \int_0^\infty dR\ \Phi(\mu, \sigma, R) \cdot I(q, R)_{\text{Particle}} \end{aligned}$$

where a_2, c_1, and c_2 are the coefficients in the Teubner-Strey-model, μ_D and σ_D are the coefficients for the Gaussian describing the diffraction peak, $\Phi(\mu, \sigma, R)$ is the aforementioned size distribution, and $I(q, R)$ is the four-shell form factor describing the scattering intensity from a P3HT:PCBM-particle described by the radius, R, as elaborated above. Finally, $C_{\text{Teubner-Strey}}$ and $C_{\text{Diffraction peak}}$ provide the relative scales for the different contributions. Note that we assume that the Teubner-Strey domains and the particle sizes are on different length scales and that we can therefor omit the crossterms, as the scattering contributions from these decouple.

The analysis was performed using the WillItFit-framework[33], and the source code for the presented models has been made available in the code repository of this software.

In the fits in figure 2, we have assumed that the polydispersity of the sample can be described as a lognormal-distribution. As part of this study, we also attempted to fit alternative distributions to the same data (e.g. a normal- and Schultz-distribution), and can report that this does not significantly change the fit or the overall refined structure.

As mentioned, the distribution from the final model shown in red in figure 1 is a log-normal distribution of the radii of the P3HT:PCBM-particles described by the median, m, and variance, s^2 :

$$m = 83.9\ Å \qquad s^2 = 0.21$$

We emphasise that the distribution describes the radii of the P3HT:PCBM-structure. In the model, the layer of SDS has a radius of 9.7 Å.

The inclusion of the Teubner-Strey-term describing the emulsion-like internal structure appears to be necessary in order to adequately describe the shoulder in the data around 0.09 $Å^{-1}$ and is consistent with the general view of the internal segregation of P3HT and PCBM[17], which would indeed be a prerequisite for the crystallinity exhibited by Landfester-particles.

From the refined parameters describing the Teubner-Strey-emulsions, one can deduce the characteristic correlation length, ξ, and the characteristic domain size, d, respectively. From the parameters describing the fit shown in figure 2, we can calculate these quantities:

$$\xi = 31.3\ Å \qquad d = 83.0\ Å$$

These values correspond well to the length-scale of the P3HT-crystallites, which was established from the width of the peak in the high-q region of the data. It is possible that the shoulder around 0.09 $Å^{-1}$ can be attributed to the small-angle scattering signal from the P3HT-domains in the Landfester-particles or PCBM rich domains in a P3HT mixture.

Other work mainly employing energy resolved X-ray absorption have found core-shell structures inside Landfester nanoparticles[13,16,34]. For those experiments the investigated Landfester particles were about ten times the size (radius of ≥ 100 nm) compared to the particles investigated in this manuscript. It is therefore not unlikely that the internal structure could be different for those two cases. However, these big particles are less interesting for organic solar cell wherein the whole active layer is only hundreds of nanometer thick.

Experiments by Richards et al.[17] used neutron scattering to select between five models for internal structure. For particles with radius of about 65 nm they also found core-shell structure inspired by Ulum et al.[16]. Given the uncertainties in the data points it is unclear how strongly they exclude their other choices of models or more advanced models. With the Teubner-Strey model it is for instance entirely possible that the many nano domains are located primarily in the centre, where they are separated by 2-3 nanometers.

The mass fraction of SDS was estimated to be less than 20% and NMR experiments confirmed that the particles themselves contained no residues of chloroform (see supporting information). SDS will naturally be detrimental to the photoelectric performance of a device, but since even the state of the SDS molecules could be changed due to hydrolysis[35] it is difficult to estimate.

Nanoparticles cast as films

Our interest is to follow the precise nanoparticle morphology when the particles are cast into a wet film that is then dried and we therefore only work with single particles and particle monolayers. To investigate the spatial particle structure we employ Atomic Force Microscopy (AFM) and scan single particles spin cast on a mica substrate. The nanoparticles have a tendency to form small aggregates and connected snakelike structures on the substrate, so the particle concentration was reduced to 6 mg/L to achieve isolated particles.

The particle height and diameter were systematically extracted from the AFM images and are shown in figure 3. The particle diameter was found to be about 13 times the particle height indicating that particles are smeared out along the substrate as part of the coating process. Similar deformation was also observed for particles dropcast on mica. Our hypothesis is that the particles are soft enough to undergo a drastic deformation regardless of coating procedure (dropcast, spincast or roll-to-roll coating). We envision the transformation as spherical particles turning into deformed disk like structure upon contact with a substrate surface with sufficient low surface energy like mica or zinc oxide, but not deforming on surfaces with high surface energy such as carbon films on TEM grids.

In the experiments we were concerned that the AFM tip might contribute to the particle deformation. This effect was tested by successively scanning the same area, and verifying that reproducible particle dimensions were obtained. We also wanted to see how tip damage would appear and subjugated a single particle to constant tip scanning for prolonged time. The particle broke up into several isolated pieces suggesting the AFM tip damage would not manifest itself like the observed deformation and contributed little to the measured particle dimensions.

Crystallinity in nanoparticle films. The AFM scans contribute little to the understanding of internal particle structure after the drastic deformation. Grazing incidence wide angle X-ray scattering (GIWAXS) was employed to investigate the crystalline texture of monolayers of P3HT:PCBM 1:1 nanoparticle cast on float glass substrate. If the structure of the nanoparticles were conserved the P3HT crystal domains would be orientated randomly, and we would expect crystallinity to be independent of substrate angle. However, we see a high degree of edge-on alignment with the substrate even before annealing at 140°C as shown in figure 3. In fact 68% of the P3HT crystal domains are oriented edge-on within ±10 degrees of the substrate normal and this number increase to 91% within ±30 degrees of the substrate normal. Annealing the film at 140°C has little effect on the overall crystal orientation.

The average crystal domain sizes are characterized by the Scherrer equation. A clear annealing effect on the crystal domain size is observed (figure 3D). Annealing causes approximately a doubling in crystal domain size from 3 to 6 nm. Compared to the nanoparticles in dispersion, the average crystal size is actually reduced from 5.1 nm to about 3 nm after coating. The particle deformation process reduces the average crystal domains size, but annealing at 140°C can restore it to about 6 nm.

Crystallinity in roll-to-roll coated nanoparticles. We have extended our analysis to include roll-to-roll coated films of nanoparticles. Scalable production of organic photovoltaics will use roll-to-roll coating instead of spin coating so our results are mainly interesting if our observation also holds for roll-to-roll coating. GIWAXS data from roll-to-roll coated samples are shown in figure 4.

As seen even when coated in thick films the crystal domains of P3HT and PCBM in the nanoparticles have a high degree of texture i.e. non-random orientation. The substrate alignment of P3HT and PCBM crystals are likely due to similar mechanisms as investigated for spin coating where substrates with low surface energies cause particle deformation and rearrangement of the materials. Accelerated drying intermediate heating steps likely also contribute to the deformation.

Even in layers beyond the first, the materials in the nanoparticles align with the surface. The exact material distribution needs to be determined in the future but one could imagine the domains observed in the mono layers continue to grow when subsequent nanoparticles deform on top and increased by annealing. Since the deformation process is not fully understood it is not clear if the layer becomes a massive solid or if a porous structure is formed as the case would be for rigid spheres.

Spatial distribution of P3HT and PCBM in films roll-to-roll coated from Landfester particles. The particle deformation and crystal orientation indicates that the particles are no longer intact in the formed films. We measured the spatial distribution of P3HT and PCBM by scanning a roll-to-roll coated sample at different energies using scanning transmission X-ray microscopy (STXM) as shown in figure 5. The relative distribution of P3HT and PCBM is found by measuring STXM images at energies near the carbon k-absorption edge and fitting linear combinations of known reference spectra like previously described[36]. The relative thickness is found from the optical density above the absorption edge.

In the material distribution, we see that phase segregation domains are larger than the original particle size (~100 nm domains vs ~20 nm particle diameter). In general the PCBM domains also appear to be forming higher peaks than the P3HT. This can be deceiving for methods without chemical contrast since the PCBM domains resemble particles on their own. The overall structure after roll-to-roll coating is therefore not a true monolayer of particles but phase separated material forming a rough surface with islands of PCBM in a homogenous film of P3HT. The large phase separation before any annealing might be a product of early separation into domains within the particles. As the particles are coated, they deform upon contact with the substrate and in the accelerated drying process domains merge to larger domains. Given the observed material redistribution, it is also not surprising that P3HT crystal units decrease in size and show strong alignment with the surface substrate.

The deformation and phase separation are undesirable for OPV since the domain sizes become too large for optimal charge separation. This could be a contributing factor to the lower performance observed for nanoparticle based devices[15,16]. Schematic overviews of the structural changes that the nanoparticle undergo when coated are illustrated in **figure 6**.

As it was apparent that the Landfester particles already have phase separated during roll-coating, devices were prepared where additional phase segregation from annealing was minimized by using a low drying temperature as shown in **table 2**. However, longer drying times at lower temperatures are not feasible for large scale production. The future paths would either be to minimize the deformation using different surfactants and surface modifications or optimize the internal particle structure towards high degree of material mixing that becomes optimal when cast instead of optimizing towards an ideal internal structure that becomes suboptimal when coated.

Experimental

Nanoparticle preparation

The nanoparticles were produce by the Landfester method[9]. 400 mg of active material was dissolved in 30 mL chloroform and mixed with 90 mL 20 g/L SDS in demineralized water. The solution was placed in a water bath and sonicated for 5 min at 500 W with a Hielsher UIP1000hd unit. Chloroform was removed by evaporation at room temperature for 24 hours. Excess SDS was removed in cellulose dialysis tubes (14000 nominal molecular weight limit) with 90 mL nanoparticle dispersion in 3 L demineralized water reservoir for 72 hours with reservoir change every 24 hours. The final dispersion was concentrated by centrifugation in Amicon Ultra Centrifugal filter units (10000 nominal molecular weight limit).

TEM

TEM imaging was performed with a JEOL 3000F equipped with a 300kV FEG and a 4k CCD (Gatan MSC). For TEM imaging a droplet of the sample suspended in water (0.06g/L) was placed on a TEM copper grid with a holey carbon film. For imaging, a 60 µm objective aperture was used to enhance contrast, and the chosen magnification combined with a CCD binning of 2 resulted in a pixel resolution of 0.4 nm. From the acquired TEM images, particle sizes were measured by manually outlining the particle perimeters, using the software ImageJ and converting the measured projected particle areas to particle diameters using a circular approximation. The measured diameters are presented in the form of particle size distributions with an optimum bin size calculated according to reference[37].

STXM

The sample was prepared by roll to roll coating[7,10] nanoparticles on top of PEDOT:PSS, submerging the film in a solution of potassium hydroxide and scraping the films onto a TEM copper grid. STXM measurements were recorded at the synchrotron facility BESSY II in Berlin, Germany, at the beamline UE46-PGM2. The sample was observed in the MAXYMUS STXM end station under high vacuum at the carbon edge (images were acquired at 282 eV, 286.2 eV, 287.5 eV and 320 eV). A step size of 20 nm was used and the X-rays were detected with a photo avalanche diode. The absorption data was converted to optical density and by fitting linear combinations of reference spectra the relative material distribution maps were produced (see previous publication[36] for P3HT and PCBM reference spectra).

DLS

1 mL of nanoparticle dispersion (1 g/L) in water were measured with a DLS unit from Malvern Instruments Ltd, Zetasizer Nano Zs with a He-Ne laser 633nm max 4mW. The size distribution was automatically extracted by second order cumulant analysis. A subsequently DLS measurement was performed on 1 mL of nanoparticle dispersion (0.06 g/L) in water on a 200SM goniometer from Brookhaven Instruments that incorporate a 632.8 nm He–Ne laser. The instrument was operated at a fixed scattering angle of 90°. The standard analysis software of the instrument was used for analyzing the correlation function using double exponential fitting, free form Contin analysis and second order cumulant analysis. Both experiments were carried out at room temperature with 5 min calibration time of the sample.

SAXS

SAXS measurements on the dispersed nanoparticles (6 g/L) were carried out at the MAXLab beamline I911-SAXS[38]. 30 mL of sample were measured in a 1 mm capillary for 60 seconds under automatic sample movement to prevent beam damage. 2% Hellmanex and demineralized water were used to rinse the sample capillary between sample changes. The particles were kept in a buffer of 0.1 M Tris, 50 mM NaCl, pH 8. For each particle type a dilution series were measured and no concentration effects were observed in the SAXS data. Background from solvent and slit scattering was corrected for by subtracting a measurement of buffer solution. For data analysis, see the main text. The experiments were carried out at room temperature.

GIWAXS

GIWAXS measurements were performed with a Rigaku RU-200 rotating Cu anode as source, operating at 50 kV, 200 mA. The X-ray beam point source was monochromatized and collimated (λ = 1.5418 Å) by a multilayer optic[39]. Spin coated samples were prepared on float glass substrate cleaned by sonication in isopropanol and 30 seconds plasma etching. 6 g/L P3HT:PCBM 1:1 nanoparticles were spin coated at 2800 rpm. Sample annealing was performed on a 140°C hotplate in ambient atmosphere. Roll to roll coated samples were fabricated by slot-die coating 60 g/L P3HT:PCBM 1:1 nanoparticles on a polyethylene terephthalate (PET) substrate as described previously[7,10]. Reference samples of P3HT, PCBM and P3HT:PCBM 1:1 blend were roll-coated from chlorobenzene on PET substrate.

AFM

AFM samples were prepared on mica substrates fastened to glass. The top layer mica was removed with tape prior to spin coating 6 mg/L P3HT:PCBM 1:1 nanoparticles at 2800 rpm. The AFM measurements were done as 5x5 micron micrographs with a 1024x1024 pixel resolution on a N8 Neos (Bruker Nano GmbH, Herzogenrath, Germany) using PPP-NCLR cantilevers (NANOSENSORS,Neuchatel, Switzerland). The AFM micrographs were post-processed with SPIP 6.2.6 software where particle height and diameter were extracted using an automated thresholding routine.

Device

A device structure of Glass/ITO/ZnO/Active layer/MoO_3/Al was used. Zinc oxide nanoparticle fabricated by the sol-gel method was spin coated at 1500 rpm onto an ITO substrate. The substrate was heated to 80°C and Landfester P3HT:PCBM 1:1 particles were spin coated at 800 rpm. The film was dried 60 min at 80°C in vacuum. About 10 nm of MoO_3 and 100 nm of Al was deposited on top of the active layer by thermal evaporation in a vacuum of 2×10^{-4} Pa. The device area was 12 mm^2. The photoelectric characterization was performed using a Keithley 236 source meter and a calibrated AM1.5G solar simulator.

Conclusions

We have characterized water based ink for organic photovoltaics fabricated as Landfester nanoparticles in dispersion. The size distribution is found to be smaller than normally reported in the literature (radii on the order of 10 nm) and in particular second order cumulant analysis of DLS data is found to overestimate the particle radius by at least 10 nm.

We have determined the internal particle structure of particles on the nanometer scale and found it is not a core-shell structure (previous found for larger particles) but a more complex intermixture of crystal P3HT or PCBM domains in a matrix of P3HT-PCBM. Crystal nano domains form within the particles given a sufficient fraction of P3HT is present. Presence of PCBM reduces the average crystal size from 8.7 nm in pure P3HT to 5 nm in a P3HT:PCBM 1:1 mix. The overall crystallinity also decreases by a factor of 2.7 in the P3HT:PCBM 1:1 particles compared to pure P3HT particles.

Upon spin and drop casting the nanoparticles deform and the average "particle" height becomes 5.2 ± 1.2 nm and the corresponding diameter about 13 times larger. The crystal domain size decreases from 5.1 nm to 3 nm and are highly textured with 91% crystals aligned edge-on (within ±30 degrees) of the substrate. Annealing at 140°C can restore the substrate aligned crystals to about 6 nm size. Face-on crystals are in general about a factor of 2 larger, which could indicate the edge-on crystals are limited by the overall particle height of 5.2 ± 1.2 nm.

After roll-to-roll coating the nanoparticles, aggregates of PCBM protrude in a homogeneous matrix of P3HT with domain sizes on approximate 100 nm. Without chemical information, such structure could easily be mistaken for intact nanoparticles. Crystal surface orientation is also observed in thicker roll coated nanoparticle layers. It is conjectured that phase segregation takes place to an extent that is harmful for the OPV power conversion efficiency.

For optimal OPV performance, crystallization and phase separation in the water-based ink presents a problem, because bulk layers traditionally are well mixed when cast and achieve optimal performance upon annealing. This could also explain why nanoparticle based devices are not able to reach the performance of annealed bulk hetero junction devices – because the nanoparticle based layers might start out with large phase segregated domains.

For future experiments it would be very interesting to investigate the effect of solvent and surfactant on internal structure and crystallization – and whether the success of surfactant free nanoparticles may be explained by a higher degree of material mixing and smaller crystal domains.

Acknowledgements

We gratefully acknowledge financial support from The Danish Council for Strategic Research through the WAPART project, and from The Danish Council for Independent Research Natural Sciences, through the DANSCATT grant. We also express our gratitude to Michael Bechtel, for kind assistance during the experiments with the STXM at MAXYMUS, BESSY II, by the MPI for intelligent systems, department Schütz. The MAX-lab synchrotron is acknowledged for providing access, beam-time, and support at the I911-4 SAXS-beamline. Specifically, we thank Dr. Søren Kynde and beam-line scientist Dr. Christopher Söderberg for their assistance during the data acquisition.

Notes and references

[a] Department of Energy Conversion and Storage, DTU, Frederiksborgvej 399, 4000 Roskilde, Denmark.
[b] Structural Biophysics, Niels Bohr Institute, Faculty of Science, University of Copenhagen, Denmark.
[c] Department of Chemistry and Bioscience, Fredrik Bajers Vej 7H, 9220, Aalborg East, Denmark.
[d] Changchun Institute of Applied Chemistry, 5625 Renmin Street, Changchun, 130022,P. R. China
† See DOI: 10.1039/b000000x/

1. R. Perez and M. Perez, *IEA SHC Sol. Updat.*, 2009, **50**, 2.
2. N. S. Lewis and D. G. Nocera, *Proc. Natl. Acad. Sci. U. S. A.*, 2006, **103**, 15729–15735.
3. C. Sener and V. Fthenakis, *Renew. Sustain. Energy Rev.*, 2014, **32**, 854–868.
4. S. B. Darling and F. You, *RSC Adv.*, 2013, **3**, 17633.
5. N. Espinosa, F. O. Lenzmann, S. Ryley, D. Angmo, M. Hösel, R. R. Søndergaard, D. Huss, S. Dafinger, S. Gritsch, J. M. Kroon, M. Jørgensen, and F. C. Krebs, *J. Mater. Chem. A*, 2013, **1**, 7037.
6. F. C. Krebs, N. Espinosa, M. Hösel, R. R. Søndergaard, and M. Jørgensen, *Adv. Mater.*, 2014, **26**, 29–39.
7. T. T. Larsen-Olsen, B. Andreasen, T. R. Andersen, A. P. L. Böttiger, E. Bundgaard, K. Norrman, J. W. Andreasen, M. Jørgensen, and F. C. Krebs, *Sol. Energy Mater. Sol. Cells*, 2012, **97**, 22–27.
8. R. Søndergaard, M. Helgesen, M. Jørgensen, and F. C. Krebs, *Adv. Energy Mater.*, 2011, **1**, 68–71.
9. K. Landfester, *Adv. Mater.*, 2001, **13**, 765–768.
10. T. R. Andersen, T. T. Larsen-Olsen, B. Andreasen, A. P. L. Böttiger, J. E. Carlé, M. Helgesen, E. Bundgaard, K. Norrman, J. W. Andreasen, M. Jørgensen, and F. C. Krebs, *ACS Nano*, 2011, **5**, 4188–96.
11. D. Darwis, D. Elkington, E. Sesa, N. Cooling, G. Bryant, X. Zhou, W. Belcher, and P. Dastoor, in *AIP Conf. Proc.*, 2011, vol. 1415, pp. 120–123.
12. S. Gärtner, M. Christmann, S. Sankaran, H. Röhm, E.-M. Prinz, F. Penth, A. Pütz, A. E. Türeli, B. Penth, B. Baumstümmler, and A. Colsmann, *Adv. Mater.*, 2014, **26**, 6653–6657.
13. K. B. Burke, A. J. Stapleton, B. Vaughan, X. Zhou, A. L. D. Kilcoyne, W. J. Belcher, and P. C. Dastoor, *Nanotechnology*, 2011, **22**, 265710.
14. D. M. DeLongchamp, R. J. Kline, and A. Herzing, *Energy Environ. Sci.*, 2012, **5**, 5980.
15. A. Stapleton, B. Vaughan, B. Xue, E. Sesa, K. Burke, X. Zhou, G. Bryant, O. Werzer, A. Nelson, A. L. David Kilcoyne, L. Thomsen, E. Wanless, W. Belcher, and P. Dastoor, *Sol. Energy Mater. Sol. Cells*, 2012, **102**, 114–124.
16. S. Ulum, N. Holmes, D. Darwis, K. Burke, A. L. D. Kilcoyne, X. Zhou, W. Belcher, and P. Dastoor, *Sol. Energy Mater. Sol. Cells*, 2013, **110**, 43–48.
17. J. J. Richards, C. L. Whittle, G. Shao, and L. D. Pozzo, *ACS Nano*, 2014, **8**, 4313–4324.
18. D. a. Shapiro, Y.-S. Yu, T. Tyliszczak, J. Cabana, R. Celestre, W. Chao, K. Kaznatcheev, a. L. D. Kilcoyne, F. Maia, S. Marchesini, Y. S. Meng, T. Warwick, L. L. Yang, and H. a. Padmore, *Nat. Photonics*, 2014, **8**, 765–769.
19. D. Beyer, W. Lebek, W. D. Hergeth, and K. Schmutzler, *Colloid Polym. Sci.*, 1990, **268**, 744–748.
20. M. Teubner and R. Strey, *J. Chem. Phys.*, 1987, **87**, 3195.
21. B. Siekmann and K. Westesen, *Colloids Surfaces B Biointerfaces*, 1994, **3**, 159–175.
22. H.-Y. Kim, J.-A. Han, D.-K. Kweon, J.-D. Park, and S.-T. Lim, *Carbohydr. Polym.*, 2013, **93**, 582–8.
23. B.-J. Kim, S.-G. Oh, M.-G. Han, and S.-S. Im, *Synth. Met.*, 2001, **122**, 297–304.
24. E. D. Gormez, K. P. Barteau, H. Wang, M. F. Toney, and Y.-L. Loo, *Chem. Commun.*, 2011, **47**, 436–438.
25. U. Holzwarth and N. Gibson, *Nat. Nanotechnol.*, 2011, **6**, 21027.
26. P. Scherrer, *Göttinger Nachrichten Math. Phys.*, 1918, **2**, 98–100.
27. M. J. Winokur, D. Spiegel, Y. Kim, A. J. Heeger, and S. Barbara, *Synth. Met.*, 1989, **28**, 419–426.
28. J. Y. Kim and C. D. Frisbie, *J. Phys. Chem. C*, 2008, **112**, 17726–17736.

29. A. P. L. Böttiger, M. Jørgensen, A. Menzel, F. C. Krebs, and J. W. Andreasen, *J. Mater. Chem.*, 2012, **22**, 22501.

30. P. E. Shaw, A. Ruseckas, and I. D. W. Samuel, *Adv. Mater.*, 2008, **20**, 3516–3520.

31. Y. Huang, Y. Liao, S. Li, M. Wu, C. Chen, and W. Su, *Sol. Energy Mater. Sol. Cells*, 2009, **93**, 888–892.

32. J. S. Pedersen, *Adv. Colloid Interface Sci.*, 1997, **70**, 171–210.

33. M. C. Pedersen, L. Arleth, and K. Mortensen, *J. Appl. Crystallogr.*, 2013, **46**, 1894–1898.

34. N. P. Holmes, K. B. Burke, P. Sista, M. Barr, H. D. Magurudeniya, M. C. Stefan, a. L. D. Kilcoyne, X. Zhou, P. C. Dastoor, and W. J. Belcher, *Sol. Energy Mater. Sol. Cells*, 2013, **117**, 437–445.

35. M. Nakagaki and S. Yokoyama, *J. Pharm. Sci.*, 1985, **74**, 1047–1052.

36. E. B. L. Pedersen, T. Tromholt, M. V. Madsen, A. P. L. Bottiger, M. Weigand, F. C. Krebs, and J. W. Andreasen, *J. Mater. Chem. C*, 2014, **2**, 5176.

37. D. Freedman and P. Diaconis, *Zeitschrift für Wahrscheinlichkeitstheorie und Verwandte Gebiete*, 1981, **57**, 453–476.

38. A. Labrador, Y. Cerenius, C. Svensson, K. Theodor, and T. Plivelic, *J. Phys. Conf. Ser.*, 2013, **425**, 072019.

39. D. Apitz, R. P. Bertram, N. Benter, W. Hieringer, J. W. Andreasen, M. M. Nielsen, P. M. Johansen, and K. Buse, *Phys. Rev. E - Stat. Nonlinear, Soft Matter Phys.*, 2005, **72**, 1–10.

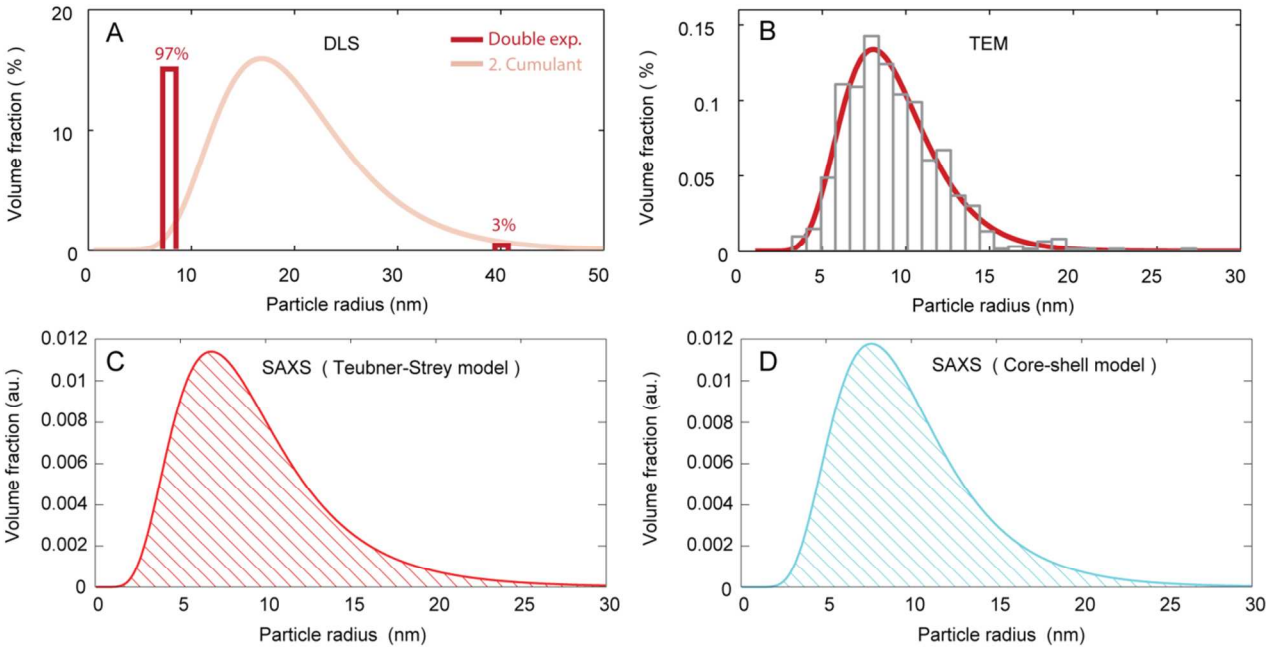

Figure 1, Size distribution of P3HT:PCBM 1:1 Landfester particles measured with different methods. A) Dynamic light scattering of particles dispersed in water. A double exponential fit to the correlation function yields 97% volume fraction of the particles have a radius of 8.9 nm in agreement with the other methods. A traditional second order cumulant analysis gives an impression of >10 nm larger particle sizes. B) Transmission Electron Microscopy of particles drop casted on a holey carbon copper grid (representative TEM images are shown in the supplementary information). C-D) Small angle X-ray scattering results from particles dispersed in water using different models for internal structure showing results according to the Teubner-Strey model in C) and a core-shell model in D). Corresponding raw SAXS data are shown in figure 2.

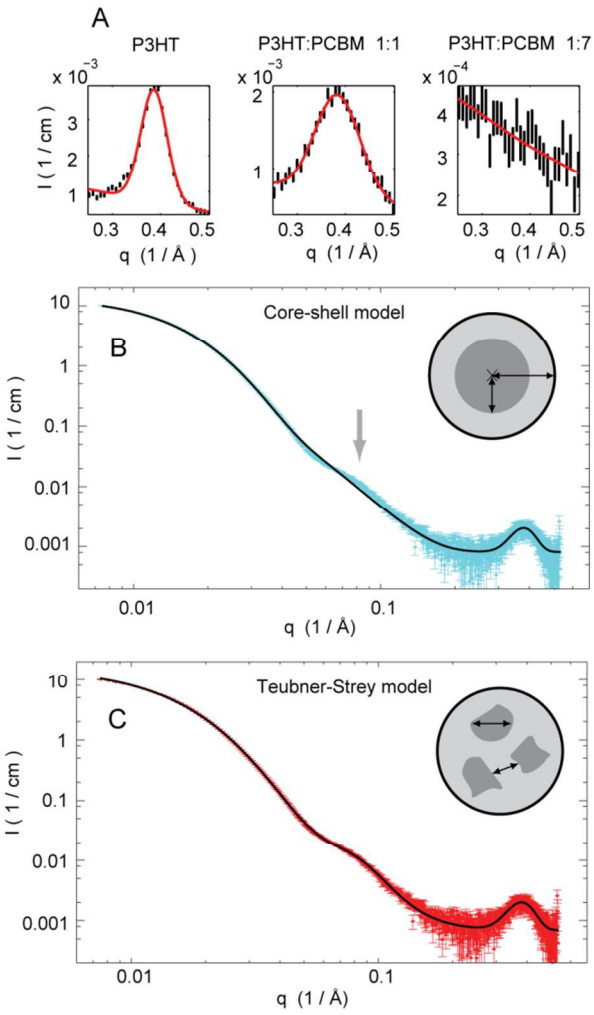

Figure 2, Small angle X-ray Scattering (SAXS) of nanoparticles dispersed in water. A) Scattering from the P3HT 100 peak for different compositions of P3HT and PCBM. B-C) Full SAXS spectrum for P3HT:PCBM 1:1 particles fitted to different internal models: B) Core-shell model (inner and outer radius) which does not fit the second shoulder around 0.08 $Å^{-1}$ marked with a grey arrow. C) Teubner-Strey model (domain size and distance) matching all features of the scattering curve.

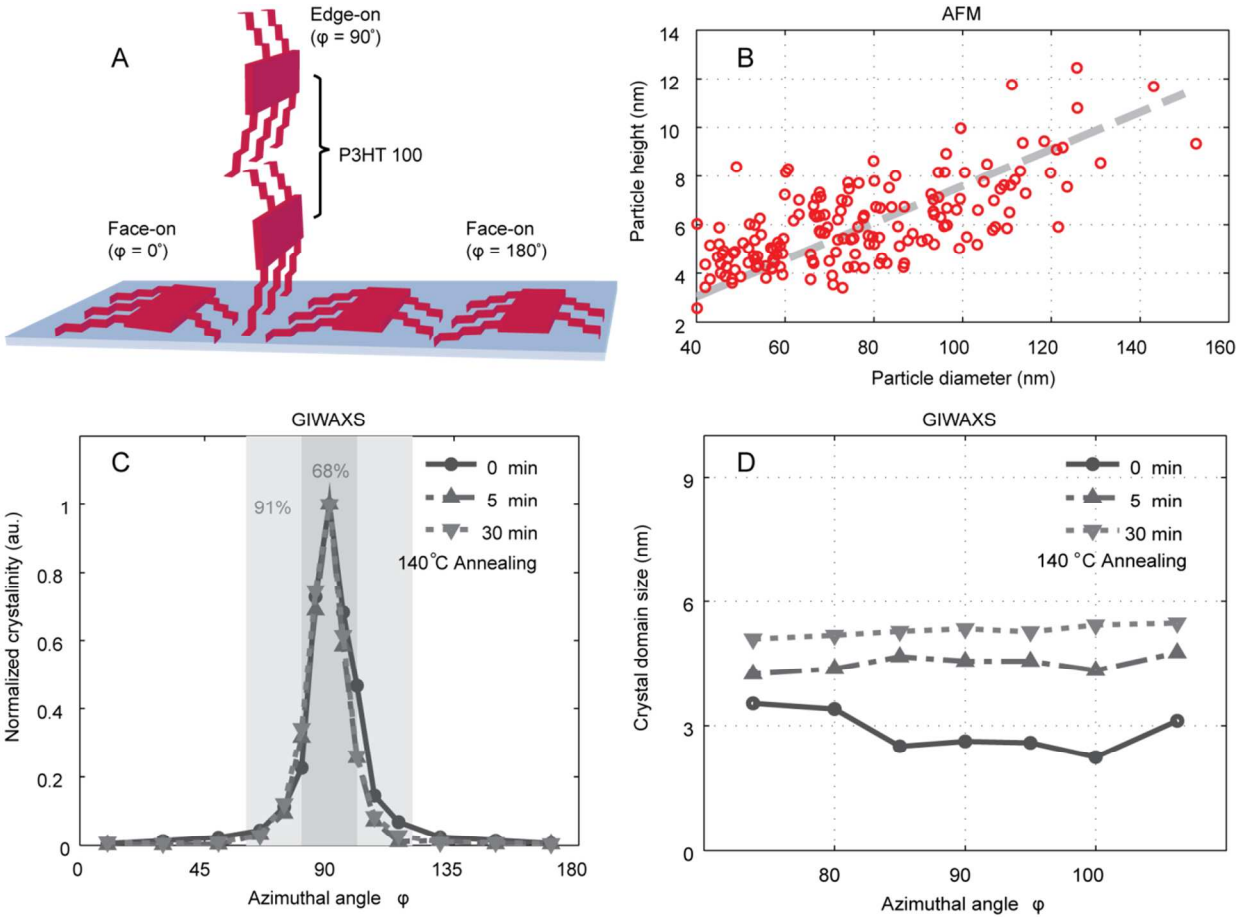

Figure 3, Particle deformation and reorientation of crystal domains. A) Schematic of face-on and edge-on orientation of P3HT. B) AFM measurements of individual P3HT:PCBM 1:1 nanoparticles spin cast on a mica substrate. The fitted trend line finds the particle diameter is about 13 times the particle height. C) Azimuthal distribution of P3HT 100 crystallinity normalized to the highest degree of crystallinity. The overall texture (angular distribution of integrated diffraction intensity) does not change as a function of annealing. Before annealing 68% of the crystallinity is aligned edge-on with the substrate (80-100 degrees azimuthal angle. D) P3HT 100 average domain size as function of azimuthal angle. The crystal domain size increases with annealing. The edge-on crystals reach a maximum of 6 nm average crystal size with annealing - about the same as the particle height found in AFM measurements. The small minority of crystals with other orientations exhibit larger domain sizes along *100,* but as their scattered intensity is very weak, the uncertainties associated with fitting are quite high and sizes are consequently not reported for these untextured crystallites (see supplementary information for more details).

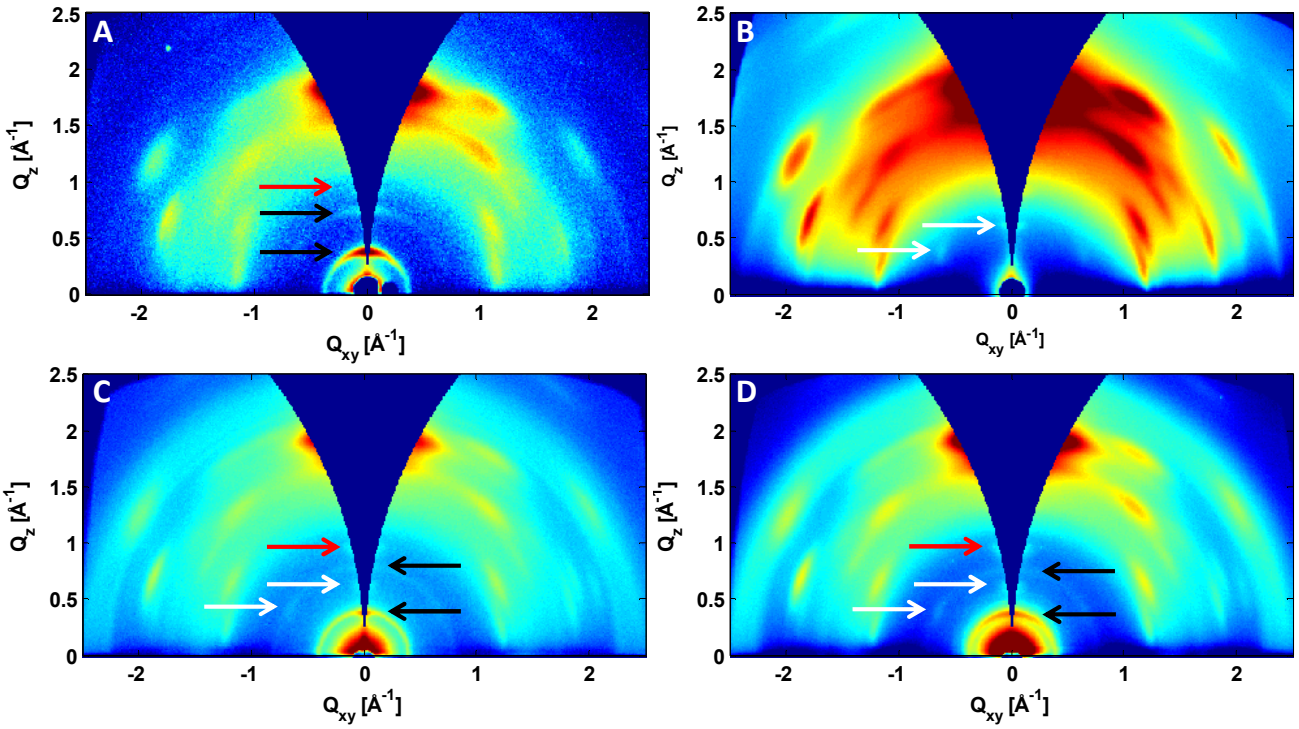

Figure 4, GIWAXS data represented in reciprocal space coordinates for A) P3HT roll-coated from chlorobenzene on PET foil B) PCBM roll-coated on PET foil C)P3HT:PCBM 1:1 blend, roll-coated from chlorobenzene on PET foil and D) P3HT:PCBM 1:1 nanoparticles roll-coated from water on PET foil. Black arrows in A, C and D show (100) and (200) reflections from textured P3HT with preferential edge-on orientation. White arrows in B, C and D show (11$\bar{1}$) and (002) reflections corresponding to textured PCBM. The high degree of textured material in the roll coated nanoparticle layer indicates the particle shape is not conserved, but particle deformation and phase segregation are observed to take place in a fashion similar to spin coated particles. The intensity at scattering vectors larger than 1 Å^{-1} is dominated by diffraction from the highly crystalline PET foil. The red arrows indicate a reflection that is also tentatively assigned to PET. See the supplementary information for details on identification and indexing of the crystalline phases.

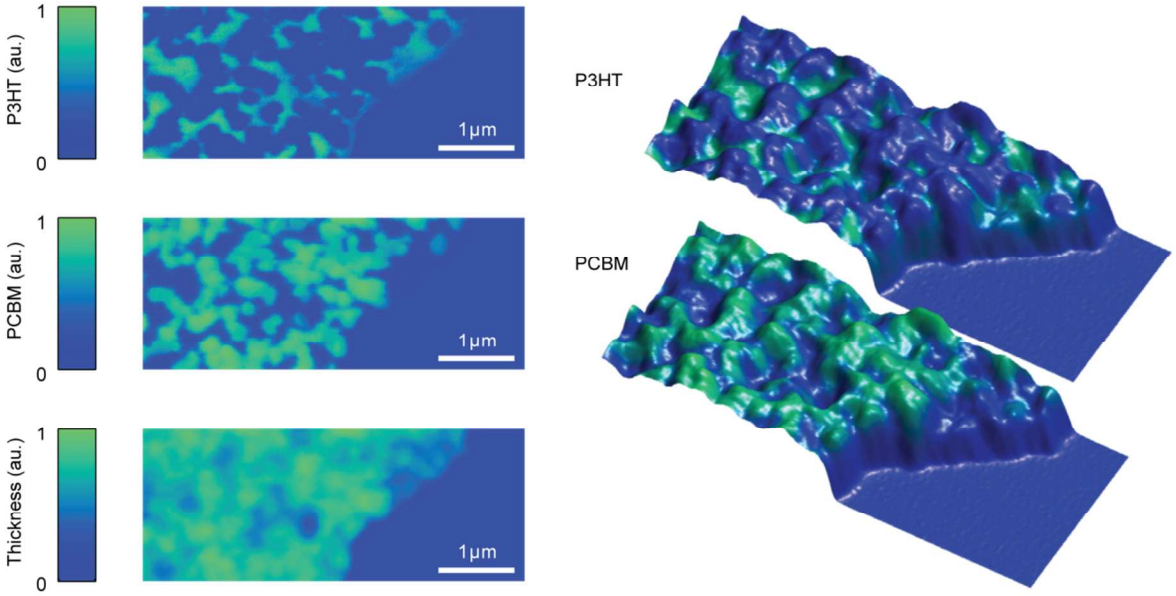

Figure 5, Spatially distibution of active material for a roll coated nanoparticle film dertermined using scaning X-ray transmission microcopy near the carbon K-edge. To the left graphs are shown with relative distribution of P3HT and PCBM as well as relative thickness found from optical density at 320 eV. Clear phase seperation is observed in domains >100 nm. To the right there are rendered thickness maps using coloring from the relative ditribution of P3HT (top) and PCBM (bottom). A clear tendency that the peak areas contain mainly PCBM appears.

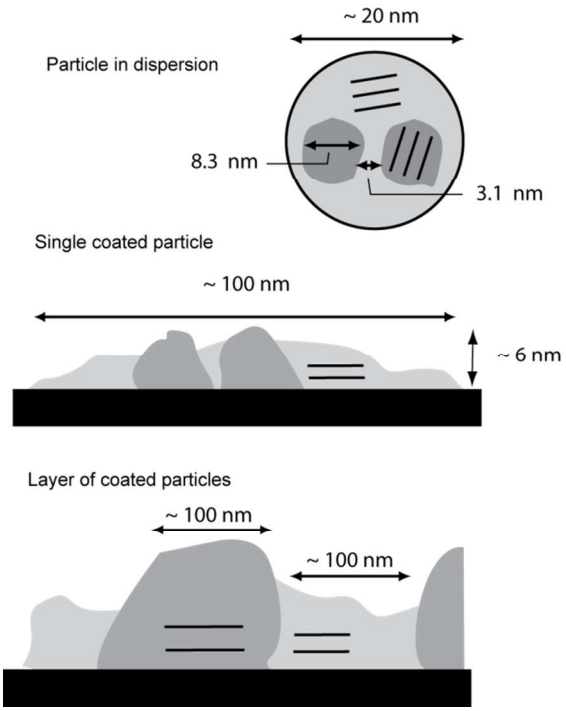

Figure 6, Schematic overview of structure and crystallinity in P3HT:PCBM 1:1 Landfester particles. They particles start out as a lognorm polydisperse size distribution ranging from 10-40 nm in diameter. The internal structure is accurately described by a Teubner-Strey model with domain sizes of about 8.3 nm separated by 3.1 nm. These domains could either be crystalline P3HT or PCBM rich areas. When an isolated particle is coated on a substrate it undergo drastic morphological changes as it is smeared out along the surface and the crystal domains decrease in size and align with the substrate. When roll-to-roll coating thicker layers, the P3HT and PCBM phase separate further and aggregate to large +100 nm domains. The majority of the crystals units also remain aligned to the substrate in the roll-to-roll coated layer.

	Domain size (nm)	Molecules per domain	Normalized crystallinity
P3HT	8.7	5.2	100 %
P3HT:PCBM 1:1	5.1	3.0	37 %

Table 1: Average P3HT crystal domain sizes and corresponding number of P3HT molecules in the average crystal unit. The crystallinity is shown relative to the crystallinity of neat P3HT nanoparticles (normalized for concentration).

	J_{sc} (mA/cm^2)	V_{oc} (V)	FF (PCE)	PCE (%)	T_{drying} (°C)
Roll to roll coated[7]	1.95	0.45	33.1	0.29	140
Spin coated	4.89	0.47	50.5	1.16	80

Table 2: Photovoltaic performance of devices with P3HT:PCBM 1:1 Landfester nanoparticles as active layer. A lower drying temperature over longer time could be applied to the spin coated devices since they were not bound to the fixed processing speed imposed by roll to roll coating.

Table of Contents

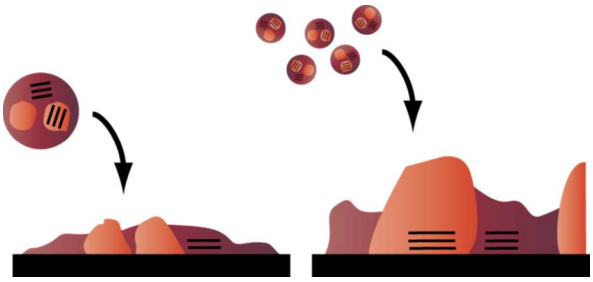

Studying water dispersible photoactive nanoparticles used for organic photovoltaics we provide new insights in the internal structure, crystallinity and the previously unreported drastic changes that occur when the particles are cast into a film.